Experimental and numerical investigation of supersonic turbulent boundary layer bleeding

Julian Giehler, Thibault Leudiere, Robert Soares, Pierre Grenson, Reynald Bur

▶ **To cite this version:**

Julian Giehler, Thibault Leudiere, Robert Soares, Pierre Grenson, Reynald Bur. Experimental and numerical investigation of supersonic turbulent boundary layer bleeding. AERO 2023 - 57th 3AF International Conference on Applied Aerodynamics, 3AF, Mar 2023, Bordeaux, France. hal-04065720

HAL Id: hal-04065720
https://hal.science/hal-04065720

Submitted on 12 Apr 2023

HAL is a multi-disciplinary open access archive for the deposit and dissemination of scientific research documents, whether they are published or not. The documents may come from teaching and research institutions in France or abroad, or from public or private research centers.

L'archive ouverte pluridisciplinaire **HAL**, est destinée au dépôt et à la diffusion de documents scientifiques de niveau recherche, publiés ou non, émanant des établissements d'enseignement et de recherche français ou étrangers, des laboratoires publics ou privés.

Association Aéronautique et Astronautique de France

57th 3AF International Conference on Applied Aerodynamics
29 — 31 March 2023, Bordeaux – France

AERO2023-75-GIEHLER

Experimental and Numerical Investigation of Supersonic Turbulent Boundary Layer Bleeding

Julian Giehler[(1)*], Thibault Leudiere[(1)], Robert Soares Morgadinho[(1)], Pierre Grenson[(1)], Reynald Bur[(1)]
[(1)] *DAAA, ONERA, Université Paris Saclay, 92190 Meudon, France*
[*] *Corresponding author: julian.giehler@onera.fr*

ABSTRACT

This study presents simulations and experiments on the effect of porous bleed systems on a supersonic turbulent boundary layer at a Mach number of M=1.6. The results indicate a good fit between the RANS simulations and the experiments based on LDV, BOS, and pressure measurements. The numerical simulations well capture the overall flow topology. Both approaches show the same trend of fuller profiles with higher suction rates. The findings suggest that RANS simulations can be used to investigate the effect of bleed systems for different bleed parameters to improve bleed models. Overall, this study provides valuable insights into the working principle of bleed systems, which are crucial for designing and optimizing supersonic air intakes.

1. INTRODUCTION

Porous bleed systems are a proven technology to control supersonic flow with and without shock-boundary layer interactions. The idea is the removal of the low-momentum flow in the vicinity of the wall to make the boundary layer more resilient against adverse pressure gradients. While the basic principle is simple, the flow physics inside the hole is difficult to understand and predict. The small size of the bleed holes, whose diameter is approximately the compressible boundary layer displacement thickness [1, 2], makes measurements inside the hole challenging, if not impossible. However, thanks to the increase in computational power in recent years, numerical simulations investigating the bleed flow became feasible [3, 4].

Even with increasing numerical resources, simulations of entire porous bleed systems are too expensive in terms of time and costs. Therefore, bleed models are required, which can be applied as a boundary condition instead of including all bleed holes in the domain. However, common bleed models [5–7] do not consider geometrical parameters which can affect the flow into the holes and inside the boundary layer [8]. Moreover, the approach of applying bleed models as a continuous boundary condition leads to an overestimation of the thinning effect [9].

Consequently, further numerical investigations are required to examine the influence of bleed parameters and improve the modeling. Nevertheless, experimental studies are needed to validate the numerical findings. Existing datasets lack in giving information about both boundary layer profiles and bleed mass flow rates. To the best of our knowledge, there is only one available experimental dataset containing bleed mass flow rate and boundary layer measurements in the case of supersonic turbulent boundary bleeding [10, 11]. Other measurements focused either on the overall flow topology [3], containing shock-boundary layer interactions [12], or using other hole geometries [13].

In this study, our existing numerical setup using three-dimensional steady-state Reynolds-averaged Navier-Stokes (RANS) simulations [8] is compared to measurements inside the boundary layer. The effect of supersonic $M = 1.6$ turbulent boundary layer bleed is investigated for different suction rates in numerical and experimental approaches.

2. METHODOLOGY

In this section, both experimental and numerical techniques are introduced. The investigated problem is the supersonic turbulent boundary layer bleeding, which is identical in both approaches. The working regime is similar to a bleed system installed upstream of a shock in a supersonic air intake.

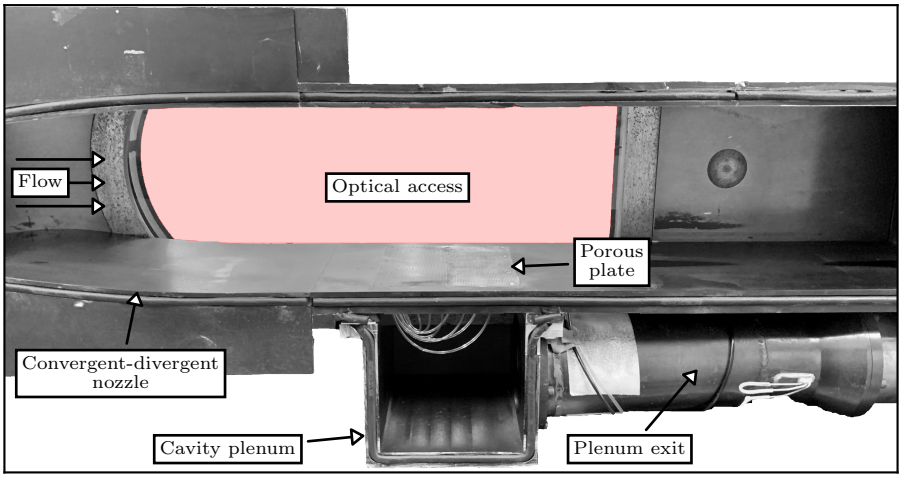

Figure 1: Experimental setup

2.1 Experimental setup

2.1.1 Wind tunnel

The experiments are performed in the continuous-running S8Ch supersonic wind tunnel of the ONERA in Meudon, supplied with dried atmospheric air. Fig. 1 shows a photograph of the test section. A convergent-divergent nozzle generates a Mach $M = 1.62$ flow. The size of the working section is 120 mm in width and 120 mm in height. The porous bleed system is installed 50 mm downstream of the nozzle exit. Windows at the side walls allow optical access to the whole test section around the bleed region.

2.1.2 Porous bleed system

The porous plate has a length of 40 mm (extendable to 80 mm) and a span of 80 mm, corresponding to 2/3 of the channel span. Preliminary numerical investigations have shown that wider plates do not affect the center flow but require higher suction rates as the suction area is increased. The utilized plate has a porosity of $\phi = 14.5\,\%$, which is a typical value for supersonic air intakes. The hole diameter is $D = 0.5$ mm, and thus slightly below the ratio $D/\delta_{1,c} = 1$. The thickness of the plate is $T = 0.5$ mm, corresponding to a thickness-to-diameter ratio of $T/D = 1$. A stiffening system inside the cavity is used to avoid the bending of the plate caused by the suction.

Moreover, the holes are distributed in a triangular shape resulting in different streamwise positions of every second column of holes. The stagger angle between the columns is $\beta = 30°$.

The bleed mass flow rate can be varied using a choked throat at the plenum exit. The throat diameter varies from $D_{pl,ex} = 10$ mm to 50 mm, while the inner pipe diameter is 76.2 mm (3 inches). Applying a discharge coefficient of $C_D = 0.95$, the bleed mass flow rate can be determined using the mass flow rate for choked nozzles.

2.1.3 Laser-Doppler-Velocimetry

A two-component Laser-Doppler-Velocimetry system is used to describe the flow field around the bleed region. Two lasers from the *Coherent Genesis MX SLM-series* with wavelengths 514.5 nm and 488 nm are utilized to measure both streamwise and wall-normal velocity components of the flow. Both fringe patterns are tilted 45° with respect to the flow to obtain the closest possible measurements to the wall. A 40 MHz frequency shift is added to one of the beams by the *FiberFlow* system from *Dantec* to resolve negative velocities.

Both emitted beams have a waist diameter of 4.3 mm. The distance between the beams is set to 35 mm, a beam expander with a ratio of 1.95, and a converging lens with a 230 mm focal length is applied. The probe volume characteristics can be calculated using classical relations [14], resulting in probe diameters of 35.04 µm/33.23 µm and probe lengths of 0.46 mm/0.44 mm. The fringe spacing is 3.39 µm/3.22 µm. With the given characteristics, sampling rates of the order of $\mathcal{O}$(1 kHz) are achieved.

2.1.4 Flow visualization

A Background Oriented Schlieren (BOS) system [15] is installed to monitor the flow in real-time. With the BOS method, the deviation of the light rays induced by density gradients is measured by cross-correlating one image of a random pattern without flow and one with the flow. The deflections in streamwise and wall-normal directions are estimated using the in-house *FOLKI* algorithm [16].

2.1.5 Pressure measurements

Static pressure measurements are performed to monitor the flow. Pressure taps on the top wall inside the convergent-divergent nozzle and the test section are used to check the correct starting of the test section. Moreover, pressure taps on the bottom wall and the porous plate are installed with an offset of 10 mm from the center plane to acquire the wall pressure changes induced by the boundary layer bleeding. Inside the cavity plenum, pressure taps on the side and bottom walls are used to measure the plenum pressure, while pressure taps upstream and downstream of the sonic throat are used to prove choking conditions.

2.2 Numerical setup

2.2.1 Geometry and mesh

The whole test section, including the convergent-divergent nozzle, is meshed using the in-house preprocessing tool and mesh-generator *Cassiopee* [17]. The mesh is fully parameterized, allowing the variation of several bleed parameters, such as the plate length, hole diameter, or plate thickness. Therefore, each hole is modeled out of five blocks using a butterfly mesh, as shown in Fig. 2. A C-grid topology around the hole walls is used to resolve the boundary layer accurately by simultaneously reducing the number of cells. The minimum wall-normal cell size is set to 0.2 µm ($y^+ \approx 1$) inside and outside the holes. A preliminary mesh sensitivity study has shown that a cell-to-cell growth ratio of maximal 1.1 is required to accurately predict the local mass flow rate passing the bleed holes. The total number of cells is 6.2 M., including the convergent-divergent nozzle, independently of the plenum pressure.

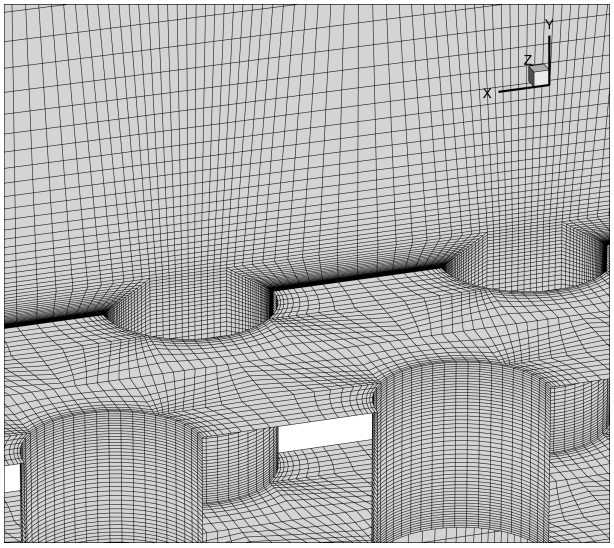

Figure 2: View on mesh around the holes

2.2.2 Flow solver

The compressible Navier-Stokes equations are numerically solved using the ONERA-Safran finite-volume solver *elsA* [18]. The Spalart-Allmaras turbulence model with quadratic constitutive relation [19] is applied. The second-order Roe upwind scheme together with the minmod limiter and the Harten entropic correction are used spatial scheme, while a backward-Euler scheme is used for the time integration. A subsonic velocity inlet condition is set upstream of the convergent-divergent nozzle. The plenum exit and the main outlet are supersonic outlets. Top and bottom walls, and all the walls around the holes are no-slip walls, while a slip-wall is applied at the plenum side walls to reduce the mesh size inside the cavity. The domain is limited using a symmetry boundary condition on the front and back.

Contrary to the experiments, the bleed mass flow rate is fixed by a choked nozzle instead of a choked throat. Therefore, the cavity plenum is prolonged, and its exit is shaped as a convergent-divergent nozzle to obtain supersonic conditions at the outlet. The size of the chocked plenum exit area $A_{pl,ex}$ is set with regard to the bleed area A_{bl}, which is the sum of all bleed hole areas $A_{bl,i}$, by introducing the throat ratio

$$TR = \frac{A_{pl,ex}}{A_{bl}} = \frac{A_{pl,ex}}{\sum A_{bl,i}}. \quad (1)$$

Fixing the throat ratio allows obtaining similar working conditions of the porous bleed, even for different plate geometries.

3. RESULTS

In the following, the experimental and numerical investigations are compared. In the first step, the flow field in the vicinity of the holes is observed. Hereafter, the boundary layer profiles are compared upstream and downstream of the bleed region.

3.1 Flow field analysis

The flow topology in the vicinity and inside the holes is shown for the simulations in Fig. 3. Following the streamlines, a deflection of the flow towards the wall is noted at the beginning of the plate as part of the boundary layer is sucked. This leads to an increase in the Mach number as the flow is accelerated. The so-called trailing shock is located at the end of the plate, where the porous plate ends, redirecting the flow in the wall-parallel direction.

Close to the wall, further expansion and shock waves are generated by the flow streaming into the holes. At each hole front, an expansion fan is located, bending the flow inside the hole. Further downstream, the barrier

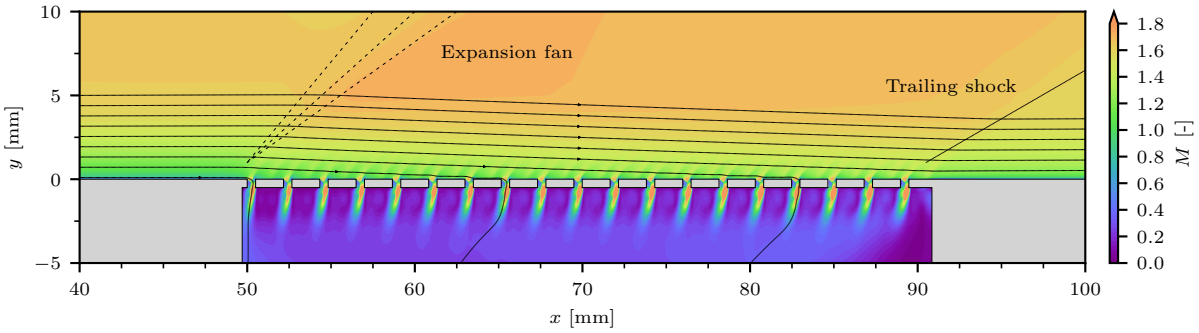

Figure 3: Mach contour field for $p_{pl}/p_t = 0.044$

shock returns the flow parallel to the wall. Inside the hole, the flow is choked, leading to a supersonic underexpanded jet into the cavity plenum.

The flow field observed using the BOS method is illustrated in Fig. 4 for a similar ratio from the cavity plenum to the total pressure of $p_{pl}/p_t = 0.044$. Both the expansion fan at the beginning of the plate and the trailing shock at the end are visible. Moreover, as the displacement d is the highest close to the wall where the density gradient is maximum, the thinning of the boundary layer is perceptible. Downstream of the bleed region, the boundary layer is significantly fuller and smaller.

On the porous plate, the effect of the hole flow is apparent. Especially for the farthest downstream located holes, the effect on the flow inside the boundary layer is observed as expansion and compression waves are evident. Since the porous plate is mounted on the floor, an overlapping of the pocket and the plate closes the holes located at the first 10 mm of the plate. Thus, no suction is present in this region, but the hole contour creates roughness. Also, a Mach wave caused by the junction from the floor to the porous plate is present. The holes downstream of the bleed region are closed with plaster, which does not affect the flow and enables measuring the boundary layer profiles in this region.

The wall pressure along the bleed region is presented in Fig. 5. On the top, the numerically extracted pressure contour on the wall is illustrated for the first bleed holes. The suction effect is evident: near the front of the holes, the pressure decreases because of the presence of an expansion fan. Further downstream, the so-called barrier shock inside the hole leads to an adverse pressure gradient resulting in a significantly higher wall pressure downstream of the hole.

For a comparison with the experiment, the wall pressure is extracted on the line between two hole columns (dotted line), where the wall is fully solid, and no hole is cut. The lower plot details the trend of the wall pressure along this line. At the beginning of the plate, where an expansion fan is located, the wall pressure drops. Along the porous plate, the pressure fluctuates caused by the flow phenomena induced by the bleed holes. However, a positive slope along the plate is notable due to the compression along the porous plate. Since the boundary layer thinning is not linear but stronger at the beginning of the plate, the flow is continuously deflected towards the wall-normal direction [8]. At the end of the bleed region, the pressure increases because of the trailing shock, resulting in a slightly increased wall pressure downstream of the plate compared to the upstream pressure.

In the experiments, the wall pressure is measured at discrete locations around and in the bleed region, as illustrated by the red points. Upstream and downstream of the bleed region, the measured wall pressure is slightly higher, which may be caused by the three-dimensionality of the flow inside the wind tunnel or Mach waves caused by the junction between the test section and the convergent-divergent nozzle. However, the deviation equals upstream and downstream, which proves the same behavior of the bleed system. Along the plate, the mea-

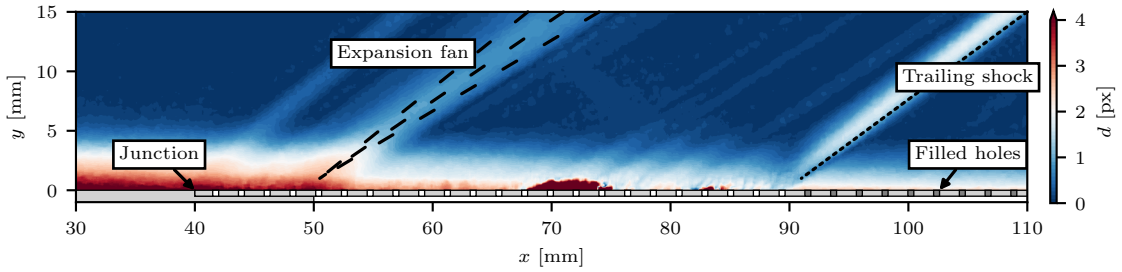

Figure 4: BOS visualization of the flow around the porous plate for $p_{pl}/p_t = 0.046$

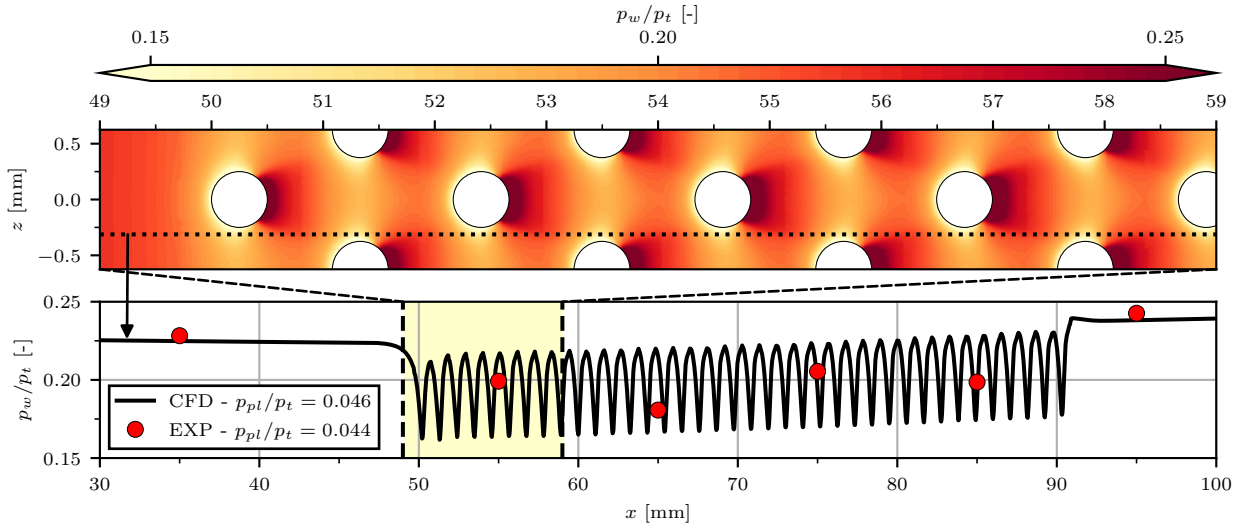

Figure 5: Static wall pressure along the bleed region

sured pressure is within the range of the pressure fluctuations. The non-steady trend of the experiments results from the diameter of the pressure taps and their positions with respect to the bleed holes. As the diameter is of the same order of magnitude as the bleed hole diameter, the pressure is averaged above a relatively large area. Depending on the position, the acquired pressure is mainly affected by the expansion fan or barrier shock and thus lower or higher.

Overall, the numerically and experimentally observed flow fields are similar. The same flow topology is apparent, and the flow is not strongly affected by any geometrical differences.

3.2 Boundary layer profiles

In the following, the boundary layer profiles are compared. Fig. 6 schematically visualizes the location of the observed profiles. The profiles are measured 15 mm upstream and downstream of the plate in both simulations and experiments. Upstream of the plate, this distance is chosen as the position is unaffected by the junction from the floor to the porous plate and the non-suction holes. Moreover, the upstream influence of the porous bleed is numerically found to be below 5 mm, which results in similar boundary layer profiles independent of the suction rate.

As described in Sec. 3.1, a trailing shock is caused by a deflection of the flow at the end of the porous bleed. Consequently, the boundary layer downstream of the bleed region is disturbed by the shock and does not allow accurate measurements. Therefore, the same distance of 15 mm is selected here. A view in Fig. 6 reveals that the boundary layer thickness is slightly lower downstream of the trailing shock. However, the sonic height is significantly lower, resulting in a fuller boundary layer.

Fig. 7 compares the velocity profile extracted from the simulation and the measured profile by means of LDV. The closest point to the wall experimentally measured is located at a wall-normal distance $y = 0.2$ mm ($y^+ \mathcal{O}(100)$). The simulation fits very well with the experimental measurements. The boundary layer thickness δ_{99} is equal in both experiments and simulations, even though the total conditions are slightly different (see Tab. 1).

The boundary layer profile extracted from the simula-

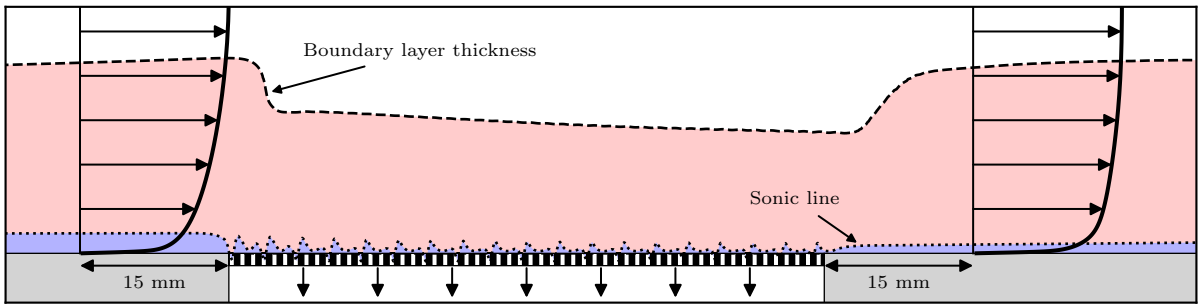

Figure 6: Illustration on the effect of the porous bleed system on the boundary layer based on numerical results

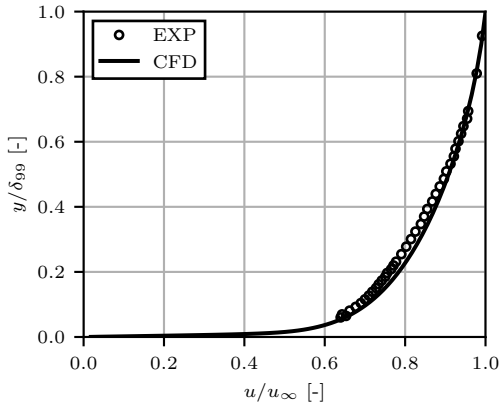

Figure 7: Comparison of the velocity profiles 15 mm upstream of the bleed region

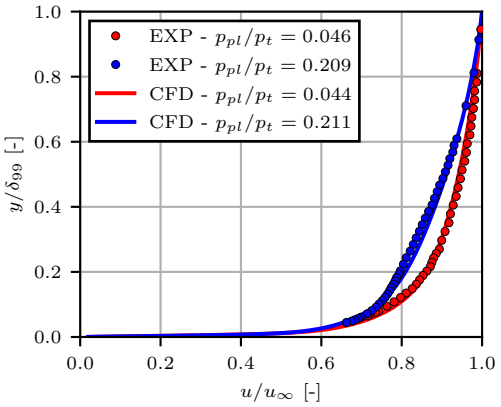

Figure 8: Comparison of the velocity profiles 15 mm downstream of the bleed region for two different pressure ratios

tions is slightly fuller than the extracted profile from the experiments. This is probably caused by the higher wall roughness in the experimental setup. However, the differences are negligibly minor.

	M	p_t	T_t	δ_{99}
Experiment	1.63	99 800 Pa	293 K	4.32 mm
Simulation	1.63	92 100 Pa	300 K	4.32 mm

Table 1: Flow properties upstream of the bleed region

With the aim of validating the simulations for different working conditions of the porous bleed, the boundary layer profiles downstream of the bleed region are measured for several suction rates. For the comparison with the simulations, the pressure inside the cavity plenum is measured. As the flow at the center plane is assumed to be two-dimensional, the ratio of plenum pressure to total pressure is more suitable than using the bleed mass flow rate, which may be affected by the three-dimensionality of the flow inside the wind tunnel close to the side walls.

The comparison of the simulations and the experiments downstream of the bleed region is detailed in Fig. 8 for the lowest and the highest suction rate. For the lowest suction rate, the plenum pressure is slightly lower than the static wall pressure inside the channel ($p_w/p_t \approx 0.226$). Both experiments and simulations show the same trend again. However, the simulations predict a slightly fuller profile which is an artifact of the fuller inflow profile. Remarkably, the boundary layer thickness is with $\delta_{99} = 4.8$ mm thicker than upstream of the bleed region, which is caused by the barrier shock.

For the highest suction rate, the holes are choked, as shown by the simulations in Fig. 3. The boundary layer profiles obtained from simulations and experiments show an almost perfect fit in this case. The boundary layer is significantly fuller than in the case of low suction rate. Also, the boundary layer is thinner than the upstream profile with $\delta_{99} = 3.7$ mm.

All experimentally acquired boundary layer profiles are compared in Fig. 9a. The significant influence of the suction rate is apparent: The higher the suction rate, the lower the pressure ratio and the fuller the boundary layer profile. A significantly fuller boundary layer is already found for the lowest suction rate. However, the suction mainly affects the lower part of the boundary layer, while the velocity is lower with further wall distance compared to the inflow. As stated before and shown in Fig. 6, the trailing shock essentially affects the boundary layer.

A further increase in the suction rate leads to an even fuller boundary layer profile. Again, the major difference is found in the near-wall region, while the outer boundary layer is mainly unaffected. For more significant suction rates, the whole boundary layer is fuller. From a pressure ratio $p_{pl}/p_t \approx 0.1$, the profiles converge, which means that the maximum effect is achieved, and a lower pressure inside the cavity does not lead to fuller profiles. This results from choking the flow inside the holes, which limits the bleed mass flow rate.

The same trends are found in the numerical simulations, as shown in Fig. 9b. Low suction rates mainly affect the near-wall region, while the outer boundary layer is unaffected. Lower pressure ratios increase the effectiveness of the porous bleed system until choking is achieved, which limits the bleed effect.

4. CONCLUSION & OUTLOOK

In this paper, we presented simulations and experiments on the supersonic turbulent boundary layer bleeding for a Mach number of $M = 1.6$. The findings indicate a very good fit between the RANS simulations and the experiments based on LDV, BOS, and pressure measurements.

In both experiments and simulations, the same flow field is found: The porous bleed system leads to a thin-

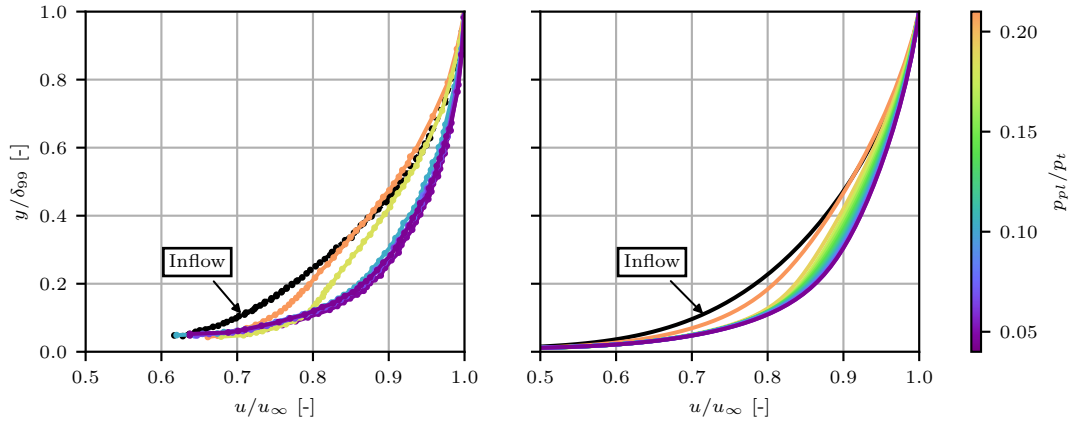

(a) Experiments (b) Simulations

Figure 9: Boundary layer profiles 15 mm downstream of the bleed region compared to the inflow

ning of the boundary layer. Consequently, an expansion fan at the beginning of the porous plate and a trailing shock at its end are present. The wall pressure along the plate is lower than the upstream pressure but increases to the end. The trailing shock induces an adverse pressure gradient, resulting in a higher wall pressure downstream of the bleed region.

Also, the boundary layer profiles are well captured by the simulations. Upstream of the bleed region, the simulated boundary layer is predicted to be slightly fuller than measured in the experiments. Downstream of the porous bleed, the fit between experiments and simulations is very good independently of the suction rate. Both approaches show the same trend of fuller profiles with higher suction rates. Moreover, the results show a near-wall effect of low suction rates, leading to fuller but slightly thicker boundary layer profiles compared to the upstream profile. With higher suction rates, the whole profile becomes fuller and thinner.

The findings of this study legitimate the use of RANS simulations to investigate the effect of porous bleed systems. As experiments are too time- and cost-intensive to examine comprehensive parametric studies, numerical simulations are required to deepen the knowledge about the working principle of bleed systems to improve bleed models.

Future work will focus on the acquisition of the flow field around the porous bleed with and without shock-boundary layer interactions. Moreover, measurements with larger hole diameters shall prove the existence of spanwise variations caused by the holes [20].

ACKNOWLEDGMENTS

This project has received funding from the European Union's Horizon 2020 research and innovation programme under grant agreement No EC grant 860909.

REFERENCES

[1] Jan Syberg and T. E. Hickcox. Design of a Bleed System for a Mach 3. 5 Inlet. Technical report, National Aeronautics and Space Administration, Washington, DC, 1973.

[2] Gary J. Harloff and Gregory E. Smith. Supersonic-inlet boundary-layer bleed flow. *AIAA J.*, 34(4):778–785, apr 1996. URL https://arc.aiaa.org/doi/10.2514/3.13140.

[3] Joseph Oorebeek, Holger Babinsky, M. Ugolotti, Paul D. Orkwis, and Sean Duncan. Experimental and Computational Investigations of a Normal-Hole-Bled Supersonic Boundary Layer. *AIAA J.*, 53(12):3726–3736, dec 2015. URL https://arc.aiaa.org/doi/10.2514/1.J053956.

[4] Gokhan Akar and Sinan Eyi. Computational Modelling and Analysis of Porous Bleed Holes at Supersonic Speeds. In *AIAA Propuls. Energy 2020 Forum*, Reston, Virginia, aug 2020. American Institute of Aeronautics and Astronautics. URL https://arc.aiaa.org/doi/10.2514/6.2020-3721.

[5] Piotr P. Doerffer and Rainer Bohning. Modelling of perforated plate aerodynamics performance. *Aerosp. Sci. Technol.*, 4(8):525–534, nov 2000. URL https://linkinghub.elsevier.com/retrieve/pii/S1270963800010634.

[6] John W. Slater. Improvements in Modeling 90-degree Bleed Holes for Supersonic Inlets. *J. Propuls. Power*, 28(4):773–781, jul 2012. URL https://arc.aiaa.org/doi/10.2514/1.B34333.

[7] Yohan Choe, Chongam Kim, and Kwanghyun Kim. Effects of Optimized Bleed System on Super-

sonic Inlet Performance and Buzz. *J. Propuls. Power*, 36(2):211–222, mar 2020. URL https://arc.aiaa.org/doi/10.2514/1.B37474.

[8] Julian Giehler, Pierre Grenson, and Reynald Bur. Parameter Influence on the Porous Bleed Performance with & without Shock-Boundary Layer Interaction. In *AIAA Aviat. 2022 Forum*, Reston, Virginia, 2022. American Institute of Aeronautics and Astronautics. URL https://arc.aiaa.org/doi/10.2514/6.2022-3239.

[9] Julian Giehler, Pierre Grenson, and Reynald Bur. Porous Bleed Boundary Conditions for Shock-Induced Boundary Layer Separation Control. In *56th 3AF Int. Conf. Appl. Aerodyn.*, Paris, 2022. Association Aéronautique et Astronautique de France.

[10] Brian Willis, David O. Davis, and Warren R. Hingst. Flow coefficient behavior for boundary layer bleed holes and slots. In *33rd Aerosp. Sci. Meet. Exhib.*, Reston, Virginia, jan 1995. American Institute of Aeronautics and Astronautics. URL https://arc.aiaa.org/doi/10.2514/6.1995-31.

[11] Brian Willis and David O. Davis. Boundary layer development downstream of a bleed mass flow removal region. In *32nd Jt. Propuls. Conf. Exhib.*, Reston, Virginia, jul 1996. American Institute of Aeronautics and Astronautics. URL https://arc.aiaa.org/doi/10.2514/6.1996-3278.

[12] Brian Willis, David O. Davis, and Warren R. Hingst. Flowfield measurements in a normal-hole-bled oblique shock-wave and turbulent boundary-layer interaction. In *31st Jt. Propuls. Conf. Exhib.*, Reston, Virginia, jul 1995. American Institute of Aeronautics and Astronautics. URL https://arc.aiaa.org/doi/10.2514/6.1995-2885.

[13] David O. Davis, Brian Willis, and Mark Schoenenberger. Porous and microporous honeycomb composites as potential boundary-layer bleed materials. In *33rd Jt. Propuls. Conf. Exhib.*, Reston, Virginia, jul 1997. American Institute of Aeronautics and Astronautics. URL https://arc.aiaa.org/doi/10.2514/6.1997-3260.

[14] F. Durst, A. Melling, J. H. Whitelaw, and C. P. Wang. Principles and Practice of Laser-Doppler Anemometry. *J. Appl. Mech.*, 44(3):518–518, sep 1977. URL https://asmedigitalcollection.asme.org/appliedmechanics/article/44/3/518/385614/Principles-and-Practice-of-LaserDoppler-Anemometry.

[15] F. Nicolas, V. Todoroff, A. Plyer, G. Le Besnerais, D. Donjat, F. Micheli, F. Champagnat, P. Cornic, and Y. Le Sant. A direct approach for instantaneous 3D density field reconstruction from background-oriented schlieren (BOS) measurements. *Exp. Fluids*, 57(1):13, jan 2016. URL http://link.springer.com/10.1007/s00348-015-2100-x.

[16] F. Champagnat, A. Plyer, G. Le Besnerais, B. Leclaire, S. Davoust, and Y. Le Sant. Fast and accurate PIV computation using highly parallel iterative correlation maximization. *Exp. Fluids*, 50 (4):1169–1182, 2011.

[17] Christophe Benoit, Stéphanie Péron, and Sâm Landier. Cassiopee: A CFD pre- and post-processing tool. *Aerosp. Sci. Technol.*, 45:272–283, sep 2015. URL http://dx.doi.org/10.1016/j.ast.2015.05.023https://linkinghub.elsevier.com/retrieve/pii/S1270963815001777.

[18] Laurent Cambier, Sébastien Heib, and Sylvie Plot. The Onera elsA CFD software: input from research and feedback from industry. *Mech. Ind.*, 14(3):159–174, jun 2013. URL http://www.mechanics-industry.org/10.1051/meca/2013056.

[19] P.R Spalart. Strategies for turbulence modelling and simulations. *Int. J. Heat Fluid Flow*, 21(3):252–263, jun 2000. URL https://linkinghub.elsevier.com/retrieve/pii/S0142727X00000072.

[20] Julian Giehler, Pierre Grenson, and Reynald Bur. A New Approach of Using Porous Bleed Boundary Conditions - Application of Local Porosity. In *23. DGLR-Fachsymposium der STAB*, Göttingen, 2022. Deutsche Strömungsmechanische Arbeitsgemeinschaft, STAB.